Rodriguez Martinez, ED.; Bernal, SA.; Provis, JL.; Gehman, JD.; Monzó Balbuena, JM.; Paya Bernabeu, JJ.; Borrachero Rosado, MV. (2013). Geopolymers based on spent catalyst residue from a fluid catalytic cracking (FCC) process. Fuel. 109:493-502. doi:10.1016/j.fuel.2013.02.053.

Geopolymers based on spent catalyst residue from a fluid catalytic cracking (FCC) process

Erich D. Rodríguez[1,2,†]*; Susan A. Bernal[2,3]; John L. Provis[2,3]; John D. Gehman[4]; José M. Monzó[1]; Jordi Payá[1]; M. Victoria Borrachero[1].

*errodnar@disca.upv.es, erichdavidrodriguez@gmail.com

[1]Instituto de Ciencia y Tecnología del Hormigón (ICITECH), Universitat Politècnica de València. Valencia 46022, Spain

[2] Department of Chemical and Biomolecular Engineering, University of Melbourne, Victoria 3010. Australia

[3]Department of Materials Science and Engineering, University of Sheffield, Sheffield S1 3JD, United Kingdom

[4] School of Chemistry and Bio21 Institute, University of Melbourne, Victoria 3010, Australia

[†]Current position: Research Fellow, Grupo de Materiales Compuestos. Universidad del Valle. Cali, Colombia

Con formato: Español (Colombia)

Con formato: Fuente: Sin Negrita, Sin Cursiva, Español (Colombia)

Con formato: Español (Colombia)

Comentario [ER1]: Should I put my current position..??

Abstract

This paper assesses the use of alkali activation technology in the valorization of a spent Fluid Catalytic Cracking (FCC) catalyst, which is a residue derived from the oil-cracking process, to produce 'geopolymer' binders. In particular, the effects of activation conditions on the structural characteristics of the spent catalyst-based geopolymers are determined. The zeolitic phases present in the spent catalyst are the main phases participating in the geopolymerization reaction, which is driven by the conversion of the zeolitic material to a highly Al-substituted aluminosilicate binder gel. Higher alkali content and SiO_2/Na_2O ratio lead to a denser structure with a higher degree of geopolymer gel formation and increased degree of crosslinking, as identified through ^{29}Si MAS NMR. These results highlight the feasibility of using spent FCC catalyst as a precursor for geopolymer production.

Keywords Geopolymer; Fluid catalytic cracking; catalyst residue, zeolites

Con formato: Justificado

1. Introduction

Catalysis is a widely used process in the petrochemical industry for the transformation of crude oil to gasoline and other fuel products, with an economic impact estimated at more than 6.3 million barrels per day in 2012 in the U.S. alone [1]. A wide range of zeolites and molecular sieves are commonly used in the fluid catalytic cracking (FCC) process, but the catalysts are degraded when in use. Partial or complete regeneration of spent FCC catalyst can be carried out in some cases, although in the longer term its continual reuse is not possible due to irreversible deactivation and structural damage to the zeolitic material. More than 400 petroleum refineries worldwide refine crude oil via fluid cracking catalytic units [2], and ~160,000 tons of spent catalyst residue are produced every year by the petrochemical industry. However, with an anticipated 5% annual increase in catalyst consumption, the spent catalyst residue may exceed 200,000 tons annually within a few years [3]. This residue mainly consists of SiO_2 and Al_2O_3, and can be considered as an agglomeration of zeolite crystals (mainly zeolite Y in the case of the material studied here) held together by an aluminosilicate matrix.

During the cracking reactions, the surface of FCC catalyst particles can be contaminated with different cations (including Ni, V, Fe, Cu and/or Na), and coke (carbon) is deposited in ppm levels or more. According to the European waste catalogue (commission 94/3EEC), spent FCC catalyst (code 160804) is classified as a non-hazardous material and has been used in landfill, as a source of SiO_2 and Al_2O_3 in the Portland cement clinkerization process [4], as a filler in asphaltic concretes [5], as a substitute for kaolin in the ceramic industry [6], as a raw material in the synthesis of some zeolites or for extraction of active Al_2O_3 [7,8], in the production of bricks through sintering processes [9], in the refractory industry [10] and as a supplementary cementitious material (SCM) in blended cement production [11–15].

The inclusion of spent FCC catalyst as an SCM in Portland cement blends can lead to an increase in the mechanical strength and the improvement of some durability properties as a consequence of its high reactivity with $Ca(OH)_2$ [12,13]. The zeolitic structures in spent FCC catalyst have the ability to

promote the formation of an Al-substituted C-S-H type gel (via the pozzolanic reaction) and/or hydrated aluminate phases [16]. The presence of some contaminants, such as Ni, can reduce the pozzolanic reactivity of the spent catalyst, and so the potential use of spent FCC catalysts in the production of Portland cement-based building materials must be very carefully assessed [14,17]. It has been reported that mechanical [18], thermal [19], and chemical treatments [20] can enhance the effectiveness of spent FCC catalyst as an SCM in ordinary Portland cement systems.

Geopolymers are materials with properties similar to those of hardened Portland cement, produced through the alkali activation of an aluminosilicate precursor [21,22]. The geopolymer structure is dominated by an aluminosilicate type gel, comparable with an amorphous zeolite structure [23]. The interest in geopolymers as a potential alternative to Portland cement has increased considerably during the last two decades, as these materials can present technical, environmental and economic advantages when compared with conventional cements. Geopolymer production is associated with lower energy consumption and lower CO_2 emissions compared with the Portland cement industry, as well as the benefit of providing a pathway to the valorization of high-volume reactive aluminosilicate industrial wastes or by-products [22].

Depending on the raw materials selected and their processing conditions, geopolymers can exhibit high compressive strengths, moderate shrinkage, and good performance when exposed to aggressive environments such as strong acids and high temperatures [23]. Industrial by-products such as fly ash from coal combustion, metallurgical slags, natural minerals including calcined clays, and volcanic ashes, have been successfully used as aluminosilicate precursors in the production of geopolymer systems [24]. However, the availability of those precursors in some parts of the world is limited, and therefore, there is an increasing need to identify different precursors with similar chemical and structural properties that can be widely available. Considering that spent FCC catalyst is a reactive aluminosilicate material which is produced in relatively high volumes and which does not currently have a direct pathway to valorization, it is likely that this material is a feasible precursor for the larger-

scale synthesis of geopolymers; it has recently been demonstrated [25] that alkali-activation might be a desirable alternative for the valorization of this by-product.

The aim of the present study is to analyze in more detail the potential application of alkali-activation of spent FCC catalyst waste to produce alternative binders, through the development of a better understanding of the structural features of a new spent FCC catalyst-based geopolymer. The effect of the alkali and silicate content in the structure of spent FCC catalyst-based geopolymers is determined using X-ray diffraction (XRD), Fourier ~~transmission~~ transform infrared spectroscopy (FTIR), solid state nuclear magnetic resonance spectroscopy (NMR), and scanning electron microscopy (SEM).

2. Experimental Program

2.1. Materials

Spent fluid catalytic cracking catalyst was supplied by BP Oil España (Castellon, Spain), and prior to activation was subjected to a mechanical treatment using a ball mill (Mill-2 Gabrielli) for 20 minutes to increase its reactivity [12,26]. Figure 1 shows the destruction of the spent fluid catalytic cracking catalyst particles as a consequence of the mechanical treatment applied. The particle size range determined by laser granulometry was 0.8-100 μm with a mean particle diameter of 17.1 μm. According to the chemical composition (table 1), the spent FCC catalyst has a SiO_2/Al_2O_3 ratio close to unity. The total silica content determined in previous studies following the procedure suggested by Payá et al [27] was 48.3%, while the reactive silica content determined by a KOH (4M) attack was 41.3%.

Figure 1. Scanning electron micrographs of A. untreated spent FCC catalyst and B. ball-milled FCC catalyst.

Table 1. Chemical composition of the spent fluid catalytic cracking catalyst used, on an oxide basis, from X-ray fluorescence analysis. LOI is loss on ignition.

The catalyst residue contains different crystalline zeolite phases, which are identifiable through XRD (Figure 2), with the use of the Powder Diffraction File (PDF) and American Mineralogist Crystal Structure Database (AMCSD) reference resources. The faujasite type-structure of dehydrated dealuminated US-Y zeolite ($|Al_{5.6}O_{22.4}|\cdot[Si_{175.7}Al_{16.3}O_{384}]$, PDF # 00-045-0112), ZSM-5 zeolite ($M_nAl_nSi_{(96-n)}O_{192}\cdot 16H_2O$; n<27; PDF # 00-044-0002) and mordenite ($(Ca,Na_2,K_2)Al_2Si_{10}O_{24}\cdot 7H_2O$; AMCSD # 0003444) were observed. Different high-temperature aluminosilicate polymorphs such as sillimanite (Al_2SiO_5; PDF # 00-038-0471), kyanite (Al_2SiO_5; PDF # 00-011-0046), and mullite ($3Al_2O_3\cdot 2SiO_2$; PDF # 00-015-0776), as well as quartz (SiO_2, PDF# 00-046-1045), were also identified. Sillimanite and kyanite are used as active fillers in catalysts in the petroleum industry [28]; non-catalytic or non-reactive alumina-silica compounds are used in the catalyst to remove carbonaceous and metallic contaminants (Ni or V) [29]. The spent FCC catalyst also has a high content of amorphous (glassy) aluminosilicate phases as a consequence of the partial destruction of the zeolite structures by the inclusion of lanthanum and titanium during catalyst synthesis [30], and also in service. Lanthanum oxide (La_2O_3, PDF #00-022-0641) and some traces of aluminum titanium silicate ($Al_4Ti_2SiO_{12}$; PDF # 00-022-0502) and anatase (TiO_2, PDF # 00-021-1272) were also identified.

As alkali activators, sodium silicate solutions were used, synthesized by blending distilled water, analytical grade sodium hydroxide pellets (NaOH; Sigma-Aldrich, Australia) and a commercial sodium silicate solution (PQ Silicates, Australia) with 28.7 wt.% SiO_2, 8.9 wt.% Na_2O and 62.4 wt.% H_2O. The proportions of water, NaOH and sodium silicate were adjusted to produce alkali activators with compositions $Na_2O\cdot rSiO_2\cdot 11H_2O$, where r = 0, 1.0, and 2.0.

2.2. Sample preparation

The spent FCC catalyst was activated with activator doses of 7 wt.%, 10 wt.% and 15 wt.% of Na_2O, relative to the mass of spent catalyst residue, and a water/catalyst residue ratio of 0.50. The mix designs are given in Table 2.

Table 2. Mix designs of geopolymer samples

The pastes were mixed for three minutes and then poured into a plastic container and sealed for curing at 40˚C for 28 days. Samples were milled, washed with acetone to halt the reaction process, and stored sealed until characterization.

2.3. Tests conducted

The reaction products, and structures of the geopolymers produced, were assessed through:

- X-ray diffraction (XRD) using a Bruker D8 Advance instrument with Ni-filtered Cu K_α radiation, with a step size of 0.020° and 4s/step.
- Fourier transform infrared (FTIR) spectroscopy via the KBr pellet technique, using a Bruker Tensor 27 spectrometer and 32 scans per spectrum. Spectra were collected in transmittance mode from 4000 to 400 cm^{-1} at a resolution of 4 cm^{-1}.
- Solid-state ^{29}Si and ^{27}Al magic angle spinning nuclear magnetic resonance (MAS NMR) spectra were obtained on a Varian Direct Drive VNMRS-600 spectrometer (14.1 T) using a MAS NMR probe for 4 mm o.d. zirconia rotors and a spinning speed of ν_R =10.0 kHz. ^{29}Si MAS NMR experiments were acquired using a pulse width of 4 μs and a relaxation delay of 20 s, and 3664-4096 scans. ^{27}Al MAS NMR experiments were conducted at 156.3 MHz on the same instrument, with a pulse width of 0.5 μs, a relaxation delay of 2 s, and 1024 scans. ^{29}Si and ^{27}Al chemical shifts are referenced to external samples of tetramethylsilane (TMS) and a 1.0 M aqueous solution of $Al(NO_3)_3{\cdot}9H_2O$, respectively.
- Scanning electron microscopy (SEM) was conducted using a FEI Quanta microscope (ESEM) with 15 kV accelerating voltage. The samples were

evaluated in low vacuum mode to enable the analysis of uncoated fracture surfaces.

3. Results and Discussion

3.1. X-ray diffraction (XRD)

The alkali-activation of the catalyst residue leads to the dissolution of the faujasite type zeolite (identified by XRD, as dehydrated, dealuminated zeolite Y), as shown in Figure 2 by the disappearance of the peaks assigned to this phase in the geopolymer samples. A higher alkalinity (lower SiO_2/Na_2O ratios) leads also to the dissolution of mordenite, whose peaks decrease with increasing alkali content. This behavior is also observed with higher SiO_2/Na_2O ratios in the silicate-activated systems.

Figure 2. X-ray diffractograms of the spent FCC catalyst based geopolymers after 28 days of curing

Some of the crystalline aluminosilicate phases identified in the unreacted spent FCC catalyst (Figure 2), such as mullite, kyanite and sillimanite, along with quartz, are observed in the geopolymer samples regardless of the activation conditions used. This is consistent with the known behavior of mullite and quartz in fly ash-based geopolymers, where these crystalline phases are seen to be unreactive [31]. However, the intensities of the peaks assigned to kyanite do decrease when the catalyst residue is activated with 15% Na_2O, especially when the SiO_2/Na_2O ratio is also high (sample 15N2).

The higher deviation of the XRD data from the baseline at increased alkali content is attributed to the formation of a highly amorphous new gel, consistent with the well-known geopolymer gel [32]. The degree of amorphicity of this gel is controlled by the degree of polycondensation and/or the SiO_2/Na_2O ratio [33]. The higher amorphicity identified in the silicate-activated systems with high alkalinity (such as 15N1 and 15N2) can contribute to enhancement of the mechanical performance according to the results previously obtained by Tashima *et al* [25]. In that study, it was identified when producing FCC catalyst-based geopolymers that increasing the hydroxide concentration and the inclusion of soluble silica in the alkali activator promotes increased compressive strength, reaching values of up to 68 MPa after 3 days of curing at 65ºC.

The absence of the diffraction peaks corresponding to the US-Y zeolite and the reduction of the mordenite peaks in the geopolymer samples, when compared with the unreacted catalyst residue (Figure 2), indicate that these phases are participating in the geopolymerization reactions. There was no new crystalline phase identified as a reaction product in the geopolymer samples. Albite, which was identified as a main crystalline phase in alkali-activated spent FCC catalyst geopolymers [25], was not identified in this study. Other products such as hydrosodalite that have been widely observed in metakaolin-based and fly ash-based geopolymers [34–36] were also not identified in these samples.

3.2. Fourier transform infrared (FTIR) spectroscopy

Infrared spectra of the unreacted spent FCC catalyst, and the alkali-activated pastes with different alkali concentrations and different SiO_2/Na_2O ratios, are shown in Figure 3. The spectra obtained were normalized in order to enable a direct comparison between the different geopolymers produced.

Figure 13. Fourier transform infrared spectra of alkali-activated spent FCC catalyst geopolymers after 28 days of curing

The band between 1200–950 cm^{-1} in the spectrum of the spent FCC catalyst residue is associated with the asymmetric stretching vibration mode of Si-O-T bonds (T: tetrahedral Si or Al), which is often called the "main band" in geopolymer spectra [37,38]. This band is centered at 1090 cm^{-1}, corresponding to the asymmetric stretching of Si-O-Si bonds, which also show resonances due to symmetric stretching and bending modes at ~800 cm^{-1} and 459 cm^{-1}, respectively [37,38]. The shoulder observed at 1185 cm^{-1} and the signal between 560-550 cm^{-1} are associated with the octahedrally coordinated aluminum present in the kyanite, mullite and sillimanite previously identified by XRD (Figure 2), and also potentially the mordenite in the spent residue, which might also contain some octahedral Al in extra-framework sites as consequence of the high temperatures to which the material is exposed during its use as a catalyst [39]. Tetrahedrally coordinated aluminum in the aluminosilicate phases is identified by the asymmetric stretch vibration of the AlO_4^- groups at 833 cm^{-1}.

The peaks located at 833, 789, 611, and 528 cm^{-1} correspond to the asymmetric, symmetric, double 6-ring and bending vibration modes of the aluminosilicate framework in dealuminated Y zeolites [40]. Additional peaks at 1078, 1176 and 1206 cm^{-1} are also observed in dealuminated Y zeolites [39], but the signals of other Si-rich phases overlap these bands in the samples studied here. Zeolites have two types of acidity: Brønsted acid sites involving hydroxyl groups, and Lewis acid sites associated with three-coordinated framework aluminum or with extra-framework Al containing species, which can be identified at ~1400-1450 cm^{-1} in the spectra in Figure 3 [41]. Brønsted sites are observed via a band at 3000 – 3500 cm^{-1} (not shown in Figure 3) and an additional band at 1632 cm^{-1}, associated with the bending vibration mode of –OH bonds in the mordenite structure [37,42]. The presence of the bands centered at ~1425 and 2360 cm^{-1} is likely to indicate the presence of some traces of ammonium cations and/or nitrile species which remain adsorbed on zeolites after its use as a catalyst [43].

3.2.1. Effect of alkali content.

The alkali activation of spent FCC catalyst leads to the destruction of the zeolitic structures according to the XRD results (Figure 2), and the development of new amorphous phases with different structural and bonding features. The main band in the spectra of the unreacted spent FCC catalyst is reduced in intensity and broadened after alkali activation at 7 wt.% Na_2O. This broad band identified in the geopolymers activated at 7 wt.% Na_2O indicates structural disorder in the silicate-aluminate network, and potentially an incomplete degree of polymerization in the geopolymer product.

However, at higher alkali concentrations (15 wt.% Na_2O), this peak is narrowed and significantly more intense as a consequence of the higher extent of dissolution of the aluminosilicate precursor, contributing more silicate and aluminate species for geopolymer gel formation. Increased alkali content leads to a shift of the main (asymmetric stretch) band in spent FCC catalyst-based geopolymers towards lower wavenumbers, as a consequence of a higher content of Al incorporation into the geopolymer gel [44]. The intensity of this main band, and the extent of the shift to lower wavenumbers, depend on the degree of crosslinking and the chemical nature of the gel framework formed during the geopolymerization [45,46]. Activation with a higher alkali concentration accelerates the dissolution of the aluminosilicate species in the precursor, which can lead to an enhanced rate of geopolymer network formation [46]. However, excess alkalinity can also lead to a reduced extent of gel deposition and/or re-dissolution of the gel, because the concentration required to achieve supersaturation in the solution phase is higher, affecting the properties of the final binder product obtained [23].

The activation process leads to a reduction in the intensities of the bands observed in the unreacted spent FCC catalyst at 460 cm^{-1}, 528 cm^{-1} and 609 cm^{-1}, which is associated with the dissolution of the zeolite phases. The geopolymer product shows new bands at ~725 cm^{-1} and ~850 cm^{-1} attributed to the stretching vibration of Si-O-Si(Al) bridges, and stretching vibration modes of AlO_4 sites, respectively [47]. The band at 725 cm^{-1} becomes stronger

and sharper at increased alkali contents (10 wt.% to 15 wt.% Na_2O), which is attributed to a higher degree of Al substitution in the Si-rich gel.

In silicate-activated systems with high alkalinity (10N1, 10N2, 15N1 and 15N2), the new band between 880 – 900 cm^{-1}, observed as a small shoulder on the main Si-O-T band, is assigned to the stretching vibration mode of Al-O bonds in condensed AlO_4^- groups. The band at ~584-590 cm^{-1} can be assigned to cyclosilicate vibrations whose intensity and width is associated with the Al and Si content in the geopolymer gel, along with the degree of structural disorder and/or deformation of the six-membered rings in the geopolymer gel structure. The fact that this band is observable and distinct indicates that the gel is relatively ordered.

The band at 1632 cm^{-1} in the spectrum of the unreacted spent FCC catalyst becomes more intense, and shifts slightly towards higher wavenumber (~1650 cm^{-1}) in the geopolymer pastes, as a consequence of the presence of more adsorbed hydroxyl groups (≡Si−OH···H_2O and ≡Al−OH···H_2O) in the geopolymer gel [48]. This band does not change significantly with alkali content.

3.2.2. Effect of silica content

The "main band" in the geopolymer spectra in Figure 3 shifts toward slightly higher wavenumber with increasing SiO_2/Na_2O ratio, regardless of the alkali content of the system. The main band for the geopolymer 15N0 (SiO_2/Na_2O ratio of 0) is centered at 1001 cm^{-1}, and shifts to 1024 cm^{-1} when an alkali activator with a SiO_2/Na_2O ratio of 2.0 is used. Similar behavior is also observed at lower alkali contents, where the main band of 10N1 at 1016 cm^{-1} shifts to 1032 cm^{-1} when the activator SiO_2/Na_2O ratio is increased from 1.0 to 2.0 (10N2). This shift in the main band is attributed to the reduced bond length and/or increasing bond angle in the Si-O-T bonds as a consequence of a higher content of SiO_2 and higher extent of crosslinking, consistent with the formation of a Si-rich gel with a reduced Al content, along with a reduction in the fraction of silicon sites with non-bridging oxygens (Q^3 sites) [45,49-51]. Additionally, the

bands at 584 and 725 cm^{-1} shift towards higher wavenumbers, which is also a consequence of the more Si-rich environment in the gel.

The band corresponding to the bending vibration mode of –OH (~1650 cm^{-1}) is shifted slightly towards lower wavenumber with an increased SiO_2/Na_2O ratio, which is attributed to a potential increase in the prevalence of the O-H···O bond interaction in the gel [52]. This could take place as the gel densifies and becomes more compact, as the O-H bonds of water molecules in the pores are forced to interact more closely with the bridging oxygen atoms of the framework.

3.3. Nuclear magnetic resonance spectroscopy (MAS NMR)

3.3.1. ^{27}Al MAS NMR

The ^{27}Al MAS NMR spectrum of the unreacted spent FCC catalyst (Figure 4) shows broad bands in the regions assigned to octahedrally (-10 to 30 ppm), pentahedrally (30 to 50 ppm) and tetrahedrally (50 to 80 ppm) coordinated Al sites. Considering that this precursor is composed of a variety of zeolite phases, along with other Al-containing minerals, as has previously been identified by XRD (Figure 2), none of these peaks can unambiguously be assigned to the contribution of a single phase.

Figure ~~3~~4. Solid state ^{27}Al MAS NMR spectra (14.1 T, ν_R = 10 kHz) of geopolymers, recorded after 28 days of curing.

The breadth of the ^{27}Al resonances in these high-resolution, high-field spectra suggests the presence of substantial amounts of disordered Al-containing phases. The spectrum of the spent FCC catalyst (Figure 4) shows somewhat

sharp, high intensity peaks at 10 ppm and 58 ppm, which are assigned respectively to the resonances of 6- and 4-coordinated aluminum species in ordered environments. These are consistent with the sillimanite [53], kyanite [54] and zeolite [55] structures identified by XRD in section 3.1. A low intensity signal at 28 ppm is also identified, which could be attributed to surface defect sites in the dehydrated dealuminated US-Y zeolite [56]. The broad signals observed between 30-50 ppm may be indicating the presence of aluminum species in a disturbed tetrahedral coordination (Al^{IV}) or penta-coordinated species (Al^{V}) [57–59].

In service in the catalytic cracking process, the FCC catalyst undergoes further hydrothermal dealumination, leading to removal of up to 90 wt.% of the tetrahedrally-coordinated aluminum from the zeolite framework, and consequently, hydroxyl groups associated with silicon replace aluminum-containing bonds [60]. These silanol groups are associated with the formation of a secondary mesopore surface and other structural defects induced by the loss of aluminum, resulting in a more potentially reactive material. The presence of distorted species containing tetrahedrally coordinated Al, as a result of the partial destruction of the framework while the material is in service as a catalyst, is consistent with the amorphous hump observed in the X-ray diffractogram of the unreacted spent catalyst (Figure 2).

Changes in the line shape of the ^{27}Al NMR spectrum after activation, compared to the unreacted spent catalyst, are a strong indication of which phases are participating in the geopolymerization reaction, and also provide a measure of the structural characteristics of the newly-formed gel. After the activation of the spent catalyst, the band at 28 ppm has almost completely disappeared as a consequence of the dissolution of the US-Y zeolite phase, independent of the alkali concentration used during the activation process, which is consistent with the results obtained by XRD (Figure 2). The spectrum also shows a decrease in the intensity of the resonance at 10 ppm, more pronounced at higher alkali contents. The dissolution of the dealuminated Y zeolite is also identified through the disappearance of the resonance attributed to octahedral Al. The low intensity remnant 6-coordinated Al band observed after alkali-activation is attributed to the residual mullite phase [61], which remains

invariant in the XRD, and therefore seems not to participate in the geopolymerization reaction process.

The narrow resonance of AlO_4 groups (58 ppm) in the spent FCC catalyst becomes broader with the alkali activation, which is associated with the formation of a highly crosslinked disordered aluminosilicate gel type, being the main reaction product in alkali-activated aluminosilicate binders [62], and consistent with the aluminosilicate (geopolymer) gel identified by FTIR and XRD above. Geopolymers with low alkali content (such as the 7N systems, regardless of SiO_2/Na_2O ratio) show only a slight shift in the Al^{VI} resonance compared with the unreacted FCC catalyst. On the other hand, at higher alkali content (especially for geopolymers 15N), the spectra exhibit a very notable decrease in the intensity of Al^{VI} sites, and a corresponding increase in Al^{IV}. This effect is identified at all SiO_2/Na_2O ratios in the 15N systems. The strong signal of this tetrahedral Al species (~58 ppm) for the 15N1 and 15N2 geopolymers indicates a very highly polymerized structure among the $Q^4(n\text{Al})$ silicate species.

3.3.1. ^{29}Si MAS NMR

^{29}Si MAS NMR spectroscopy was carried out for two selected silicate-activated systems, and the unreacted FCC residue (Figure 5). The spent catalyst contains silica and alumina present within various phases, such as zeolites and other aluminosilicate minerals, and thus a wide range of silicon environments can be identified as discussed throughout this study. The spectrum of the unreacted spent FCC catalyst is consistent with the presence of highly dealuminated zeolites (peak at -107 ppm), and also contains a distribution of $Q^3(n\text{Al})$ and $Q^4(n\text{Al})$ sites, with n between 0 and 4 [63], as well as sites where the Si is associated with octahedral as well as tetrahedral sites, as in the mullite, kyanite and sillimanite structures. The narrow resonance at -107 ppm is mainly attributed to the $Q^4(0\text{Al})$ sites of the US-Y zeolite [64]. Although a resonance in this position can also be attributed to quartz, the absence of this peak in the spent catalyst-based geopolymers, and the XRD results (Figure 2) where the US-Y zeolite is not observed and the small amount of quartz present

is still identified in activated pastes, it is likely that the intensity of these peaks is mainly contributed by the remnant US-Y zeolite. Given the extremely slow relaxation times of ^{29}Si in quartz (T_1 values on the order of an hour have been measured for quartz in the instrument used here, compared to the recycle delay of 20 s used here), it is likely that any quartz sites remained close to saturated throughout the experiment, and thus contributed very little to the measured spectra.

Figure 45. Solid state ^{29}Si MAS NMR spectra (14.1 T, ν_R = 10 kHz) of geopolymers recorded after 28 days of curing

The broad resonance centered at around -113 ppm is in agreement with the resonances typically identified in mordenite [65], ZSM-5 zeolite [66], as well as highly dealuminated US-Y zeolite (steamed at high temperature) [64]. According to Klinowski *et al.* [65], the $Q^4(3Al)$, $Q^4(2Al)$ and $Q^4(1Al)$ sites from the amorphous component of deactivated zeolite phases composing the spent FCC catalyst should be located at -94.5, -101.5 and -103 ppm, respectively. The high concentration of Q^4 species is coherent with the high intensity of the bands identified in the FTIR spectra (Figure 3) at 1090 cm^{-1} and 459 cm^{-1}. A site at around -87 ppm is able to be assigned to several of the different aluminosilicate polymorphs identified by XRD: mullite, sillimanite and kyanite. While this site cannot be assigned to an individual silicon environment in these materials, it best is described as an sillimanite-type site, where the SiO_4 tetrahedron is surrounded by three AlO_4 and one AlO_6 polyhedra [54,67]. This is consistent with the mullite, sillimanite and kyanite structures as identified by XRD (Figure 2), and the presence of the 4-coordinated and 6-coordinated Al sites identified in the ^{27}Al MAS NMR of the alkali-activated catalyst residue (Figure 4).

As a function of the degree of dealumination of the zeolites, the formation of terminal hydroxyl groups in environments such as $Si(OSi)_3OH$ and $Si(OSi)_2(OH)_2$ species (Q^3 and Q^2 sites respectively) can be promoted at the outer surface or internal defect sites [55]. While it is difficult to clearly

523 distinguish these sites in the spectrum of the unreacted spent catalyst, it is
524 likely that these sites make a small contribution to the broad resonance
525 identified in the spectra in Figure 5 between -90 and -100 ppm.
526
527 The alkali-activation of the spent catalyst promotes the formation of an intense,
528 asymmetric broad band centered at -92 ppm, associated with the formation of
529 an aluminosilicate type gel. In the 7N2 geopolymers, a shoulder is observed in
530 the region between -100 ppm and -120 ppm, attributed to the Q^4 sites of the
531 remnant dealuminated zeolites from the spent catalyst that have not been
532 completely consumed during the geopolymerization reaction. Taking into
533 account the XRD results (Figure 2), it is likely that US-Y zeolite contributions
534 are not observed in this region, as it seems that this phase is consumed during
535 the geopolymerization reaction even at low alkalinity conditions. The
536 resonances in the region between -80 ppm and -100 ppm are assigned to the
537 $Q^4(n\text{Al})$ sites of the newly formed geopolymer gel, consistent with the formation
538 of a three dimensional highly crosslinked type gel, as previously observed by
539 ^{29}Si MAS NMR in other low-calcium geopolymers [68] These results are
540 consistent with the trends observed by FTIR in these samples, as higher
541 wavenumbers of the FTIR bands attributed to the T-O-T bonds are identified at
542 higher alkali content (Figure 3).
543
544 The spectrum of the geopolymer sample formed at higher alkali content (15N2)
545 shows a reduction in the intensity of the shoulder between -100 ppm and -120
546 ppm, as observed in the 7N2 geopolymers. This suggests a higher extent of
547 dissolution of the dealuminated zeolite phases of the spent catalyst at higher-
548 alkalinity activation conditions, as was suggested from the FTIR results in
549 Figure 3. Additionally, the spectrum of 15N2 is slightly narrowed compared to
550 that of the 7N2 geopolymer, indicating a higher degree of ordering of the
551 aluminosilicate type gel formed at higher alkalinity conditions, which has also
552 been identified in the ^{27}Al MAS NMR results (Figure 4) via the sharpening of the
553 4-coordinated Al band at increased alkalinity. There is a slight increment in
554 the intensity in the region between -80 ppm and -100 ppm in the 15N2
555 spectrum compared to the 7N2 binders, as a consequence of the higher degree
556 of Al incorporation in the aluminosilicate gel. This is consistent with the

increased intensity of the Al^{IV} region in the 15N2 geopolymers in Figure 4, and the increased intensity of the FTIR band at 725 cm^{-1} in Figure 3, at higher alkaline contents.

The spectra of reacted and unreacted spent FCC catalyst materials could not be deconvoluted into component Gaussian peaks for quantification of the component peaks, as the remnant spent FCC catalyst in the geopolymer samples contributes to the spectrum in the region consistent with $Q^4(3Al)$, $Q^4(2Al)$ and $Q^4(1Al)$ sites. This region thus overlaps with the highly crosslinked sites in the geopolymer gel formed, making it impossible to predict which particular sites within the unreacted spent catalyst dissolve faster than others, as it is unknown whether the amorphous component of the remnant precursor embedded in the geopolymer binders is in a gel type structure or in a glass type structure, and also whether there is any Al^{VI} present within this amorphous component. Further research therefore needs to be conducted in this area before spectral deconvolution could be reliably conducted.

3.4. Scanning electron microscopy (SEM)

Figure 6 shows SEM images of spent catalyst based geopolymers formulated with different alkali concentrations and an SiO_2/Na_2O molar ratio of 1.0. The images show morphological differences in the gels formed, as a function of alkalinity. The geopolymers show a rough, heterogeneous structure, and the presence of partially reacted FCC catalyst particles (compare to unreacted particles in Figure 1), which leads to the formation of a spongy structure at low alkali content (7N1). This is probably less desirable in terms of binder performance and permeability than the denser and more homogeneous structure of the 15N1 binder. The more homogeneous structure for 15N1 is consistent with the higher dissolution and polymerization degree identified above, which leads to the formation of an aluminosilicate gel product with a higher cross-linking degree [69].

Figure ~~5~~6. Scanning electron micrographs of pastes with different alkali content (A. 7N1, B. 10N1, and C. 15N1) after 28 days of curing.

Figure 7 shows micrographs of the fracture surfaces of spent FCC catalyst-based geopolymers activated with 15 wt.% Na_2O, with different SiO_2/Na_2O ratios. The silicate-activated systems (Figure 7B,C) exhibit a denser gel structure with fewer large interconnected pores, as well as fewer unreacted particles from the aluminosilicate precursor. It is expected that the improvement in structural homogeneity of the geopolymers promotes the development of improved performance and enhanced durability as observed in [25], and consistent with results obtained in other geopolymer systems based on different aluminosilicate precursors, such as metakaolin [68] and fly ashes [35]. The increase in the silica content from system 15N1 to 15N2 does not show to promote significant differences in the gel structure, but the less favorable rheology of the highest-silica system seems to have led to the inclusion of a greater number of relatively large air bubbles in this specimen.

Figure ~~6~~ 7 Scanning electron micrographs of pastes with different SiO_2/Na_2O ratio (A. 15N0, B. 15N1, and C. 15N2) after 28 days of curing.

4. Conclusions

This study has demonstrated the potential of a zeolite-based spent fluid catalytic cracking catalyst as an effective precursor for the production of geopolymer binders. In these systems, the remnant dealuminated zeolites in the unreacted spent residue are readily dissolved, even when activation is carried out under relatively low alkalinity conditions, indicating the high reactivity of this precursor during the alkali-activation reaction. Increased alkali contents lead to the formation of a highly dense and crosslinked aluminosilicate type gel, when compared with the gels formed at lower alkali content, which were enriched in Si and present a rather heterogeneous structure with interconnected pores. This is related to the high alkalinity

required to promote the dissolution of the AlO_4^- species from the distorted zeolite structures and other phases present in the spent catalyst. This is consistent with the fact that independent of the alkali content, an increased reactive SiO_2/Al_2O_3 ratio promotes the formation of highly crosslinked Si-enriched type gels with low Al content. This work then provides the basis for further developments in this area, as a means of valorizing spent fluid catalytic cracking catalyst residues into useful geopolymer materials.

Acknowledgments

This study was sponsored by research scholarship BES-2008-002440 and EEBB-2011-43847 from the *Ministerio de Ciencia y Tecnología* of Spain, the European regional development fund (FEDER), and the *Universitat Politècnica de València* (Spain). The participation of SAB and JLP was funded by the Australian Research Council through the Discovery Projects program, and also including partial funding through the Particulate Fluids Processing Centre, a Special Research Centre of the ARC. The authors wish to acknowledge the Advanced Microscopy Facility at The University of Melbourne for assistance with the electron microscopy experiments conducted in this study.

5. References

[1] EIA Independent Statistics & Analysis, U.S. Energy Information Administration. Short-term energy outlook. September 2012.

[2] Speight J G. The chemistry and technology of petroleum (4th edition). CRC Press. Taylor & Francis Group, LLC. New York. 2006.

[3] Marafi M, Stanislaus A, Furimsky E. Handbook of spent hydroprocessing catalysts: Regeneration, rejuvenation, reclamation, environment and safety. 1st edition. ISBN: 978-0-444-53556-6. Elsevier. Amsterdam, The Netherlands 2010.

[4] Schreiber R, Yonley G. The use of spent catalyst as a raw material substitute in cement manufacturing, ACS Petrol Chem Div Preprints 1993;38:97-9.

[5] Lin J, Tarn J, Yu D, Hsiao L. Utilization of ROC spent catalyst on asphalt concrete. In: International Conference on Industrial Waste Minimization, Taiwan; 1995, p. 667-74.

[6] Escardino A, Amoros J, Moreno A, Sanchez E. Utilizing the used catalyst from refinery FCC units as a substitute for kaolin in formulating ceramic frits. Waste Manag Res 1995;13:569-78.

[7] Basaldellaa EI, Torres RM, Conconi MS. Conversion of exhausted fluid cracking catalysts into zeolites by alkaline fusion. Appl Clay Sci 2009;42:611-4.

[8] Al-Sheeha H, Marafi M, Stanislaus A. Reclamation of alumina as boehmite from an alumina-supported spent catalyst. Int J Miner Process 2008;88:59-64.

[9] Sun DD. Stabilization treatment for reutilization of spent refinery catalyst into value-added product. Energ Source 2003;25:607-15.

[10] Stonys R, Pundiene I, Antonovic V, Goberis S, Aleknevicius M. The effect of waste oil-cracking catalyst on the properties of MCC-type castable. Mater Sci-Medzg 2008;14:59-62.

[11] Pacewska B, Wilińska I, Kubissa J. Use of spent catalyst from catalytic cracking in fluidized bed as a new concrete additive, Thermochim Acta 1998;322:175-81.

[12] Payá J, Monzó J, Borrachero MV. Fluid catalytic cracking catalyst residue (FC3R): An excellent mineral by-product for improving early-strength development of cement mixtures. Cement Concrete Res 1999;29:1773-9.

[13] Chen H-L, Tseng Y-S, Hsu K-C. Spent FCC catalyst as a pozzolanic material for high-performance mortars. Cement Concrete Compos 2004;26:657-64.

[14] Dweck J, Pinto CA, Buchler P. Study of a Brasilian spent catalyst as cement aggregate by thermal and mechanical analysis. J Therm Anal Calorim 2008;92:121-7.

[15] García de Lomas M, Sánchez de Rojas M, Frías M. Pozzolanic reaction of a spent fluid catalytic cracking catalyst in FCC-cement mortars. J Therm Anal Calorim 2007;90:443-7.

[16] Glasser FP, Zornoza E, Garcés P, Payá J, Brew DRM. Pozzolanic activity of a spent fluid catalytic cracking catalyst residue. Adv Cem Res 2011; 23:105-11.

[17] Bayraktar O. Bioleaching of nickel from equilibrium fluid catalytic cracking catalysts. World J Microb Biot 2005;21:661-5.

689 [18] Pacewska B, Wilinska I, Bukowska M, Blonkowski G, Nocun-Wczelik W. An attempt to
690 improve the pozzolanic activity of waste aluminosilicate catalyst. J Therm Anal Calorim
691 2004;77:133-42.

692 [19] Hsu K-C, Tseng J-S., Ku F-F, Su N. Oil cracking waste catalyst as an active pozzolanic
693 material for superplasticized mortars. Cement Concrete Res 2001;31:1815–20.

694 [20] Payá J, Monzó J, Borrachero MV, Velázques S. Chemical activation of pozzolanic
695 reaction of fluid catalytic cracking catalyst residue in lime pastes. Adv Cem Res
696 2004;16:123-30.

697 [21] Roy DM. Alkali-activated cements Opportunities and challenges. Cement Concrete Res
698 1999;29:249-54.

699 [22] van Deventer JSJ, Provis JL, Duxson P. Technical and commercial progress in the
700 adoption of geopolymer cement. Miner Eng 2012;29:89-104.

701 [23] Provis JL, van Deventer JSJ. Geopolymers. Structure, processing, properties and industrial
702 applications. Woodhead Publishing, Cambridge; 2009.

703 [24] Duxson P, Provis JL. Designing precursors for geopolymer cements. J Am Ceram Soc
704 2008;91:3864-9.

705 [25] Tashima MM, Akasaki JL, Castaldelli VN, Soriano L, Monzó J, Payá J, et al. New
706 geopolymeric binder based on fluid catalytic cracking catalyst residue (FCC). Mater Lett
707 2012;80:50-52.

708 [26] Payá J, Monzó J, Borrachero MV, Velázquez S, Bonilla M. Determination of the
709 pozzolanic activity of fluid catalytic cracking residue. Thermogravimetric analysis studies
710 on FC3R–lime pastes. Cement Concrete Res 2003;33:1085-91.

711 [27] Payá J, Monzó J, Borrachero MV, Mellado A, Ordoñez LM. Determination of amorphous
712 silica in rice husk ash by a rapid analytical method, Cement Concrete Res
713 2001;31(2):227-31.

714 [28] Kolesnikov IM, Frolova IN. Production and activity of sillimanite and sillimanite-zeolite
715 aluminosilicate catalyst. J Appl Chem USSR 1982;55:561-71.

716 [29] Reagan WJ, White DW, Schultz WR, Jarnagin LA, Pitts F. Mullite/silica contact material,
717 its production, and its use in selective vaporization of petroleum feedstock, European
718 Patent EP 0185551; 1986.

719 [30] Liu C, Deng Y, Pan Y, Zheng S, Gao X. Interactions between heavy metals and clay
720 matrix in fluid catalytic cracking catalysts. Appl Catal A-General 2004; 257:145-50.

721 [31] Fernández-Jiménez A, Delatorre A, Palomo A, Lopezolmo G, Alonso M, Aranda M.
722 Quantitative determination of phases in the alkali activation of fly ash. Part I. Potential ash
723 reactivity. Fuel 2006;85:625-34.

724 [32] Rahier H, Mele B, Biesemans M, Wastiels J, Wu X. Low-temperature synthesized
725 aluminosilicate glasses. J Mater Sci 1996;31:71-79.

726 [33] Rahier H, Simons W, Van Mele B, Biesemans M. Low-temperature synthesized
727 aluminosilicate glasses: Part III Influence of the composition of the silicate solution on
728 production, structure and properties. J Mater Sci 1997;32:2237-47.

729 [34] De Silva P, Sagoe-Crenstil K. Medium-term phase stability of $Na_2O–Al_2O_3–SiO_2–H_2O$
730 geopolymer systems. Cement Concrete Res 2008;38:870-6.

731 [35] Criado M., Fernández-Jiménez A, de la Torre A, Aranda M, Palomo A. An XRD study of
732 the effect of the SiO_2/Na_2O ratio on the alkali activation of fly ash. Cement Concrete Res
733 2007;37:671-9.

734 [36] van Deventer JSJ, Provis JL, Duxson P, Lukey GC. Reaction mechanisms in the
735 geopolymeric conversion of inorganic waste to useful products. J Hazard Mater
736 2007;139:506-13.

737 [37] Farmer VC. The infrared spectra of minerals, Royal Society, London; 1974.

738 [38] Gadsden JA. Infrared spectra of minerals and related inorganic compounds, Butterworth,
739 London, U.K.; 1975.

740 [39] Bugaev LA, van Bokhoven JA, Sokolenko AP, Latokha YV, Avakyan LA. Local structure
741 of aluminum in zeolite mordenite as affected by temperature. J Phys Chem B
742 2005;109:10771-10778.

743 [40] Miessner H, Kosslick H, Lohse U, Parlitz B, Tuan VA. Characterization of highly
744 dealuminated faujasite-type zeolites: ultrastable zeolite Y and ZSM-20. J Phys Chem
745 1993;97:9741-8.

746 [41] Masukawa T, Komatsu T, Yashima T. Alkylation of toluene on HSAPO-5 with various Si
747 concentrations. Zeolites 1997;19:429-33.

748 [42] Li B, González RD. An in situ DRIFTS study of the deactivation and regeneration of
749 sulfated zirconia. Catal Today 1998;46:55-67.

750 [43] Damjanović L, Auroux A. Determination of acid/base properties by temperature
751 programmed desorption (TPD) and adsorption calorimetry, in: A.W. Chester, E.G.
752 Derouane (Eds.), Zeolite Characterization and Catalysis, Springer Netherlands; 2010: p.
753 107-67.

754 [44] Flanigen EM. Structural analysis by infrared spectroscopy. In: Zeolite Chemistry and
755 Catalysis. American Chemical Society, 1976; ACS Monograph Series, Washington, D.C.

756 [45] Rees CA, Provis JL, Lukey GC, van. Deventer JSJ. Attenuated total reflectance Fourier
757 transform infrared analysis of fly ash geopolymer gel aging. Langmuir 2007;23:8170-9.

758 [46] Rees CA, Provis JL, Lukey GC, van Deventer JSJ. In Situ ATR-FTIR study of the early
759 stages of fly ash geopolymer gel Formation. Langmuir 2007;23:9076-82.

760 [47] Lecomte I, Henrist C, Liégeois M, Maseri F, Rulmont A, Cloots R. (Micro)-structural
761 comparison between geopolymers, alkali-activated slag cement and Portland cement. J
762 Eur Ceram Soc 2006;26:3789-97.

763 [48] Zhang Z, Wang H, Provis JL, Bullen F, Reid A, Zhu Y. Quantitative kinetic and structural
764 analysis of geopolymers. Part 1. The activation of metakaolin with sodium hydroxide,
765 Thermochim Acta 2012;539:23-33.

766 [49] Fernández-Jiménez A, Palomo A. Mid-infrared spectroscopic studies of alkali-activated
767 fly ash structure. Micropor Mesopor Mater 2005;86:207-14.

768 [50] Fernández-Jiménez A, Palomo A, Sobrados I, Sanz J. The role played by the reactive
769 alumina content in the alkaline activation of fly ashes. Micropor Mesopor Mater
770 2006;91:111-9.

771 [51] Devine RAB. Ion implantation- and radiation-induced structural modifications in
772 amorphous SiO_2. J Non-Cryst Solids 1993;152:50-58.

773 [52] Liu X. Infrared and Raman spectroscopy, in: A.W. Chester, E.G. Derouane (Eds.), Zeolite
774 Characterization and Catalysis, Springer Netherlands, 2010: p. 197-222.

775 [53] He H, Guo J, Zhu J, Yuan P, Hu C. ^{29}Si and ^{27}Al MAS NMR spectra of mullites from
776 different kaolinites. Spectrochim Acta A 2004;60:1061-4.

777 [54] Hartman JS, Sherriff BL. Silicon-29 MAS NMR of the aluminosilicate mineral kyanite:
778 residual dipolar coupling to aluminum-27 and nonexponential spin-lattice relaxation. J
779 Phys Chem 1991;95:7575-9.

780 [55] Engelhardt G, Lohse U, Samoson A, Mägi M, Tarmak M, Lippmaa E, High resolution ^{29}Si
781 NMR of dealuminated and ultrastable Y-zeolites. Zeolites 1982;2:59-62.

782 [56] Behera B, Ray SS. Structural changes of FCC catalyst from fresh to regeneration stages
783 and associated coke in a FCC refining unit: A multinuclear solid state NMR approach.
784 Catal Today 2009;141:195-204.

785 [57] Engelhardt G, Michel D. High-resolution solid-state NMR of silicates and zeolites, John
786 Wiley and Sons, New York; 1987.

[58] Chen T-H, Houthoofd K, Grobet PJ, Toward the aluminum coordination in dealuminated mordenite and amorphous silica–alumina: A high resolution ^{27}Al MAS and MQ MAS NMR study. Micropor Mesopor Mater 2005;86:31-7.

[59] Rocha J, Carr SW, Klinowski J. ^{27}Al quadrupole nutation and ^{1}H-^{27}Al cross-polarization solid-state NMR studies of ultrastable zeolite Y with fast magic-angle spinning. Chem Phys Lett 1991;187:401-8.

[60] Rakiewicz EF, Mueller KT, Jarvie TP, Sutovich KJ, Roberie TG, Peters AW. Solid-state NMR studies of silanol groups in mildly and highly dealuminated faujasites. Micropor Mater 1996;7:81-8.

[61] Merwin LH, Sebald A, Rager H, Schneider H. ^{29}Si and ^{27}Al MAS NMR spectroscopy of mullite. Phys Chem Miner 1991;18:47-52.

[62] Duxson P, Lukey GC, Separovic F, van Deventer JSJ. Effect of alkali cations on aluminum incorporation in geopolymeric gels. Ind Eng Chem Res 2005;44:832-9.

[63] Fyfe BCA, Thomas JM, Klinowski J, Gobbi GC. Magic-angle-spinning NMR (MAS-NMR) spectroscopy and the structure zeolites. Angew Chem Int Ed 1983;22:259-75.

[64] Gore KU, Abraham A, Hegde SG, Kumar R, Amoureux J-P, Ganapathy S. MAS / 3Q-MAS NMR Studies of High Silica USY Zeolites. J Phys Chem B 2002;106:6115-20.

[65] Barras J, Klinowski J, Mccomb DW. ^{27}AI and ^{29}Si Solid-state NMR Studies of dealuminated mordenite. J Chem Soc Faraday Trans 1994:90:3719-23.

[66] Klinowski J. Recent Advances in Solid-State NMR of Zeolites. Annu Rev Mater Sci 1988;18:189-218.

[67] Jaymes I, Massiot D, Coutures J-P. Evolution of the Si environment in mullite solid solution by ^{29}Si MAS-NMR spectroscopy. J Non-Cryst Solids 1996;204:125-34.

[68] Duxson P, Provis JL, Lukey GC, Separovic F, van Deventer JSJ. ^{29}Si NMR study of structural ordering in aluminosilicate geopolymer gels. Langmuir 2005;21:3028-36.

[69] Duxson P, Provis JL, Lukey GC, Mallicoat SW, Kriven WM, van Deventer JSJ. Understanding the relationship between geopolymer composition, microstructure and mechanical properties. Colloids Surfaces A 2005;269:47-58.

Con formato: Normal (Web), Sangría: Izquierda: 0 cm, Sangría francesa: 1,13 cm, Interlineado: Múltiple 1,3 lín.

818 Table 1. Chemical composition of the spent fluid catalytic cracking catalyst
819 used, on an oxide basis, from X-ray fluorescence analysis. LOI is loss on
820 ignition.

Compound	Wt.%
SiO_2	46.94
Al_2O_3	48.40
Fe_2O_3	0.59
CaO	0.11
MgO	0.17
SO_3	0.02
K_2O	0.02
Na_2O	0.31
TiO_2	1.20
P_2O_5	0.01
Nd_2O_3	0.04
V_2O_5	0.01
La_2O_3	1.36
CeO_2	0.12
Pr_2O_3	0.19
LOI (950˚C)	0.50

821
822

823

824 Table 2. Mix designs of geopolymer samples

Geopolymer	Alkali content (wt.% Na_2O)	SiO_2/Na_2O molar ratio in alkali activator
7N0	7	0
7N1	7	1.0
7N2	7	2.0
10N0	10	0
10N1	10	1.0
10N2	10	2.0
15N0	15	0
15N1	15	1.0
15N2	15	2.0

825

826

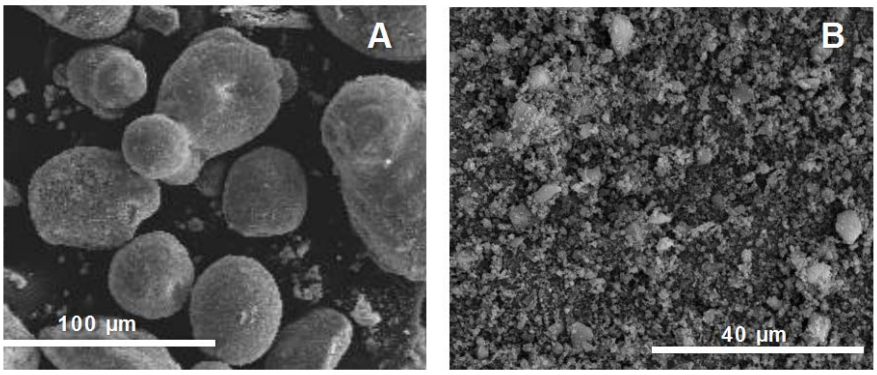

827
828
829 Figure 1. Scanning electron micrographs of A. untreated spent FCC catalyst
830 and B. ball-milled FCC catalyst.
831

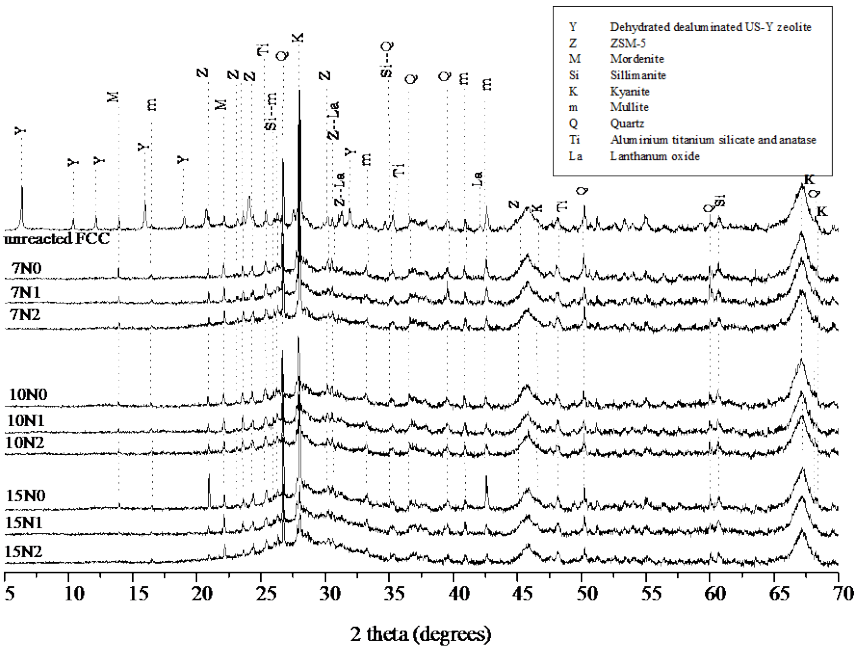

832

833 Figure 2. X-ray diffractograms of the unreacted spent FCC catalyst and
834 geopolymers produced after 28 days of curing

835

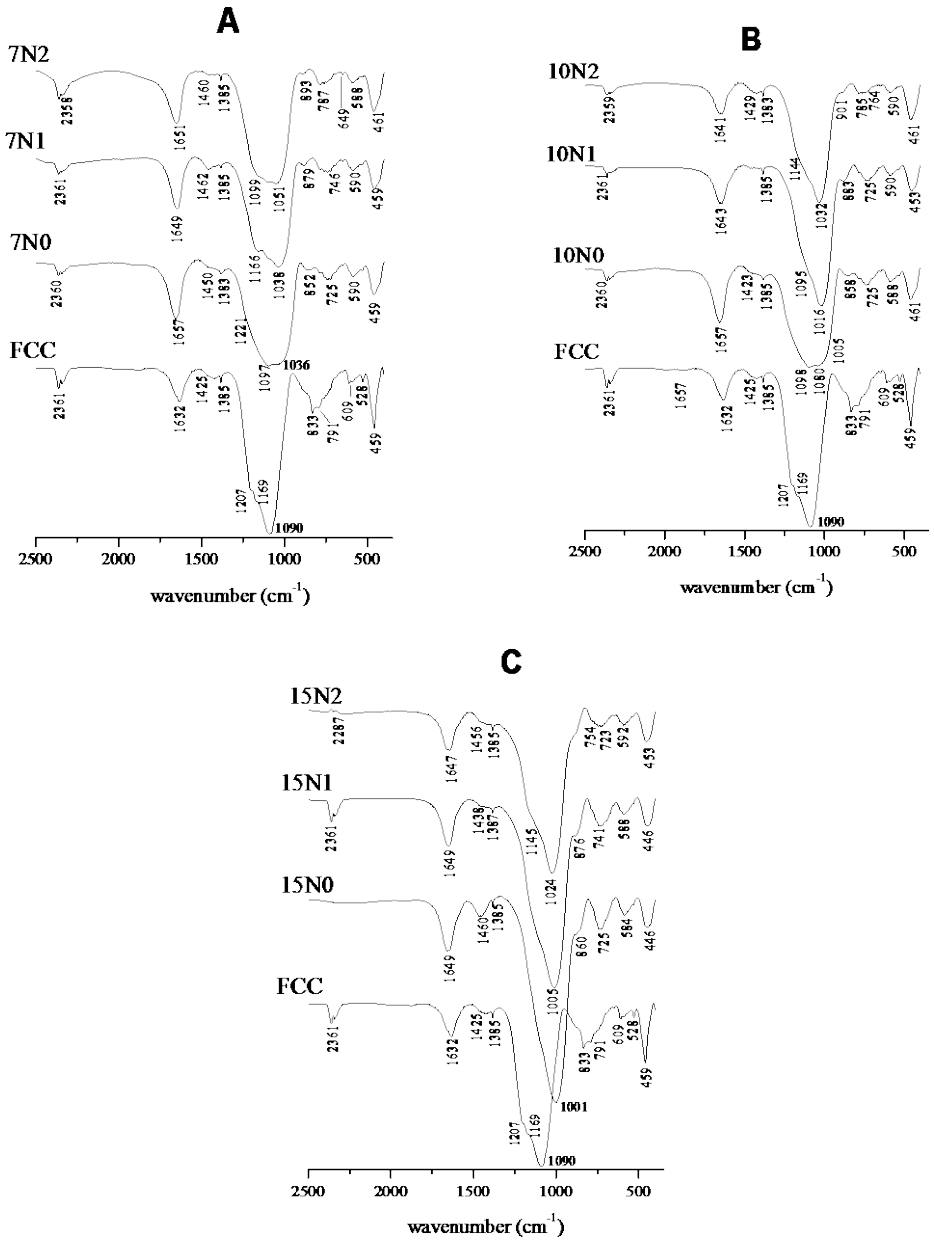

Figure 3. Fourier transform infrared spectra of alkali-activated spent FCC catalyst geopolymers after 28 days of curing.

837

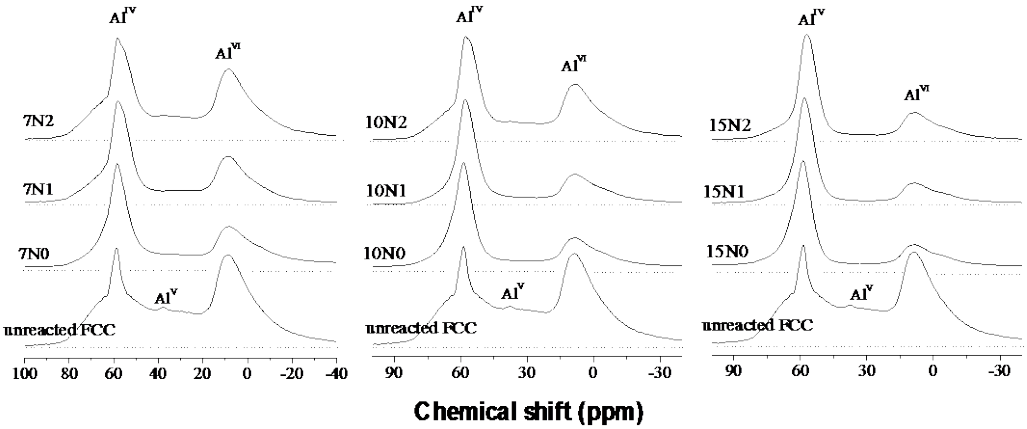

838

839 Figure 4. Solid state ^{27}Al MAS NMR spectra (14.1 T, ν_R = 10 kHz) of
840 geopolymers, recorded after 28 days of curing.

841

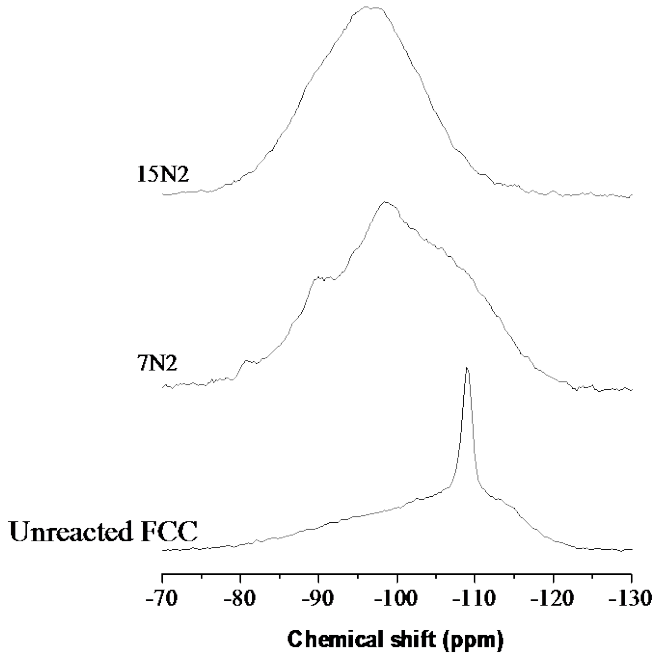

842

843

844 Figure 5. Solid state ^{29}Si MAS NMR spectra (14.1 T, ν_R = 10 kHz) of
845 geopolymers recorded after 28 days of curing

846

847 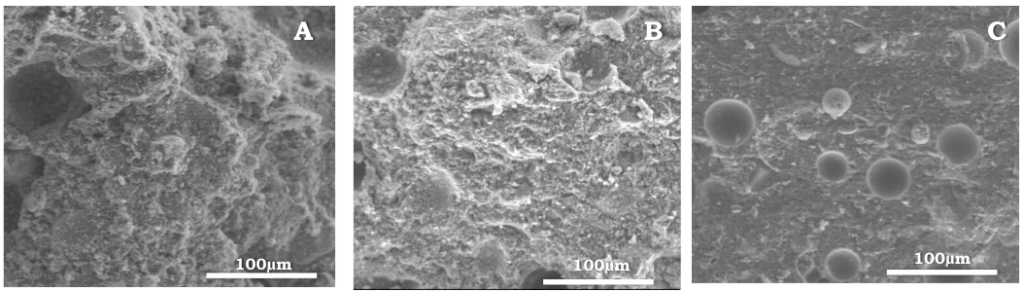

848 Figure 6. Scanning electron micrographs of pastes with different alkali content
849 (A. 7N1, B. 10N1, and C. 15N1) after 28 days of curing.
850

851

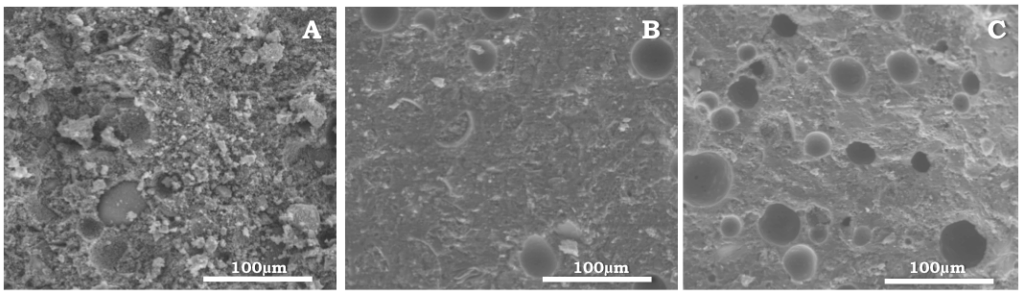

Figure 7. Scanning electron micrographs of pastes with different SiO_2/Na_2O ratio (A. 15N0, B. 15N1, and C. 15N2) after 28 days of curing.